

Radiographic-Deformation and Textural Heterogeneity (r-DepTH): An Integrated Descriptor for Brain Tumor Prognosis

Prateek Prasanna¹(✉), Jhimli Mitra¹, Niha Beig¹, Sasan Partovi², Gagandeep Singh¹, Marco Pinho³, Anant Madabhushi¹, and Pallavi Tiwari¹

¹ Case Western Reserve University, Cleveland, USA
prateek@case.edu

² University Hospitals, Cleveland, USA

³ University of Texas Southwestern Medical Center, Dallas, USA

Abstract. Most aggressive tumors are systemic, implying that their impact is not localized to the tumor itself but extends well beyond the visible tumor borders. Solid tumors (e.g. Glioblastoma) typically exert pressure on the surrounding normal parenchyma due to active proliferation, impacting neighboring structures and worsening survival. Existing approaches have focused on capturing tumor heterogeneity via shape, intensity, and texture radiomic statistics within the visible surgical margins on pre-treatment scans, with the clinical purpose of improving treatment management. However, a poorly understood aspect of heterogeneity is the impact of active proliferation and tumor burden, leading to subtle deformations in the surrounding normal parenchyma distal to the tumor. We introduce radiographic-Deformation and Textural Heterogeneity (r-DepTH), a new descriptor that attempts to capture both intra-, as well as extra-tumoral heterogeneity. r-DepTH combines radiomic measurements of (a) subtle tissue deformation measures throughout the extra-tumoral surrounding normal parenchyma, and (b) the gradient-based textural patterns in tumor and adjacent peri-tumoral regions. We demonstrate that r-DepTH enables improved prediction of disease outcome compared to descriptors extracted from within the visible tumor alone. The efficacy of r-DepTH is demonstrated in the context of distinguishing long-term (LTS) versus short-term (STS) survivors of Glioblastoma, a highly malignant brain tumor. Using a training set ($N = 68$) of treatment-naive Gadolinium T1w MRI scans, r-DepTH achieved an AUC of 0.83 in distinguishing STS versus LTS. Kaplan Meier survival analysis on an

Research was supported by 1U24CA199374-01, R01CA202752-01A1, R01CA208236-01A1, R21CA179327-01, R21CA195152-01, R01DK098503-02, 1C06-RR12463-01, PC120857, LC130463, the DOD Prostate Cancer Idea Development Award, W81XWH-16-1-0329, the Case Comprehensive Cancer Center Pilot Grant, VelaSano Grant from the Cleveland Clinic, I-Corps program, Ohio Third Frontier Program, and the Wallace H. Coulter Foundation Program in the Department of Biomedical Engineering at Case Western Reserve University. The content is solely the responsibility of the authors and does not necessarily represent the official views of the National Institutes of Health.

independent cohort ($N=11$) using the r-DepTH descriptor resulted in $p=0.038$ (log-rank test), a significant improvement over employing deformation descriptors from normal parenchyma ($p=0.17$), or textural descriptors from visible tumor ($p=0.81$) alone.

1 Introduction

Cancer is not a bounded, self-organized system. Most malignant tumors have heterogeneous growth, leading to disorderly proliferation well beyond the surgical margins. In fact, in solid tumors, depending on the malignant phenotype, the impact of the tumor is observed not just within the visible tumor, but also in the immediate peritumoral, as well as in seemingly normal-appearing adjacent field. The phenomenon of tumor involvement outside of the visible surgical margins is known as “*tumor field effect*” [1]. One largely unexplored aspect of tumor field effect in solid tumors, is the impact on overall survival due to the pressure exerted on the surrounding normal parenchyma caused by active proliferation and tumor burden thereof. For instance, in Glioblastoma (GBM), the herniation or gross distortion of the brainstem (remote to the tumor location) was identified as the proximal cause of death in 60% of the studies [2].

In this work, we present a new prognostic image-based descriptor: radiographic-Deformation and Textural Heterogeneity (r-DepTH). r-DepTH attempts to comprehensively capture the systemic nature of the tumor by computing radiomic measures of intra-, and extra-lesional texture and structural heterogeneity. Specifically, r-DepTH computes measurements from the entire tumor field as observed on MRI scans by, (1) capturing uneven yet subtle tissue deformations in the normal-appearing parenchyma, and (2) combining these tissue deformations with 3D gradient-based texture features [3] computed within the tumor confines. We demonstrate that this combination of deformation and textural heterogeneity via r-DepTH enables improved prediction of disease outcome compared to radiomic descriptors extracted from within the visible tumor alone.

2 Previous Work and Novel Contributions

Multiple studies [4–6] have explored radiomic (co-occurrence, gray-level dependence, directional gradients, and shape-based) descriptors obtained from the tumor confines on radiographic imaging (i.e. MRI, CT), to capture intra-tumoral heterogeneity. Interestingly, a recent study in GBM demonstrated that radiomic features from peri-tumoral regions were significantly more prognostic of overall patient survival than the features from within the tumor confines [7]. Similarly, the tumor field effect in GBM has been shown to be manifested several millimeters distal to the visible tumor margins [8]. These findings then beg the question if there is prognostic information that could be mined from the subtle deformations due to tumor proliferation and burden, in the seemingly normal parenchyma distal to tumor boundaries. Similarly, one could further argue that these extra-tumoral deformations (Fig. 1(c), (g)), when combined with textural

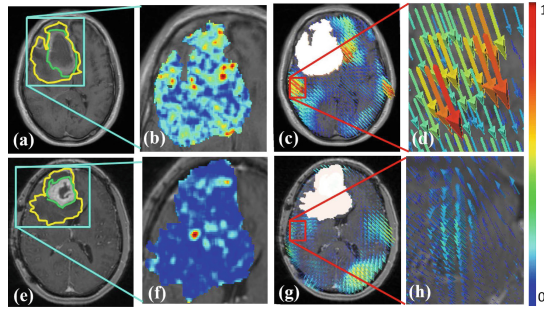


Fig. 1. Textural differences within the tumor for two different patients with (a) STS, and (e) LTS are shown in (b) and (f). Corresponding deformation magnitudes in the surrounding normal parenchyma are shown in (c), (g), and are highlighted for a small region outside the tumor across STS (d) and LTS (h).

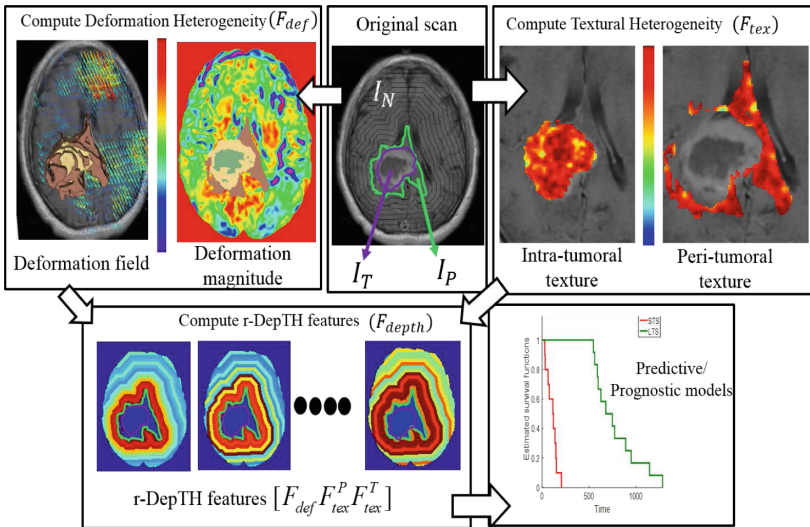


Fig. 2. Overview of r-DepTH and overall workflow.

patterns (Fig. 1(b), (f)) from the tumor confines, could potentially allow for a more comprehensive characterization of tumor heterogeneity, as compared to features from tumor alone. This integrated descriptor could then serve as a powerful prognostic marker to reliably predict patient survival in solid tumors (Fig. 2).

Uniquely, r-DepTH descriptor captures heterogeneity in solid tumors, both from intra, as well as extra-tumoral field. Firstly r-DepTH captures the textural heterogeneity from the tumor (\mathbb{F}_{tex}^T) and peritumoral regions (\mathbb{F}_{tex}^P) using the method presented in [3]. Secondly, it captures the deformation heterogeneity (\mathbb{F}_{def}) within the normal parenchyma as a function of the distance from the tumor margins. The r-DepTH descriptor is then obtained as $\mathbb{F}_{depth} =$

$[\mathbb{F}_{tex}^T, \mathbb{F}_{tex}^P, \mathbb{F}_{def}]$. r-DepTH is modeled around the rationale that highly aggressive solid tumors (with worse outcome) likely proliferate in a more disorderly fashion, and hence lead to more heterogeneous deformations in the surrounding normal parenchyma [9] (Fig. 1(c)) and higher textural heterogeneity within the tumor confines (Fig. 1(b)), as compared to relatively less aggressive tumors with overall improved outcomes. In this work, we will evaluate the utility of the r-DepTH descriptor in the context of distinguishing long-term (LTS) versus short-term (STS) GBM survivors using a total of 79 T1-w MRI patient scans.

3 Methodology

3.1 Notation

We define an image scene \mathcal{I} as $\mathcal{I} = (C, f)$, where \mathcal{I} is a spatial grid C of voxels $c \in C$, in a 3-dimensional space, \mathbb{R}^3 . Each voxel, $c \in C$ is associated with an intensity value $f(c)$. \mathcal{I}_T , \mathcal{I}_P and \mathcal{I}_N correspond to the intra-tumoral, peri-tumoral, and surrounding normal parenchyma sub-volumes within every \mathcal{I} respectively, such that $[\mathcal{I}_T, \mathcal{I}_P, \mathcal{I}_N] \subset \mathcal{I}$. We further divide the sub-volume \mathcal{I}_N into uniformly sized annular sub-volumes \mathcal{I}_N^j , where j is the number of uniformly-sized annular bands, such that $j \in \{1, \dots, k\}$, and k is an user-defined proximity parameter dependent on the distance g from the tumor margin.

3.2 Radiographic-Deformation and Textural Heterogeneity (r-DepTH) Descriptor

1. **Extraction of deformation heterogeneity descriptors from within the normal parenchyma:** Healthy T1w MNI atlas (\mathcal{I}_{Atlas}) is used to measure the tissue deformation in the normal appearing brain regions of every patient volume \mathcal{I} . \mathcal{I}_{Atlas} is first non-rigidly aligned to \mathcal{I} using mutual information based similarity measure provided in ANTs (Advanced Normalization Tools) SyN (Symmetric Normalization) toolbox [10]. The tumor mask $\hat{\mathcal{I}}_{mask}$ is removed from \mathcal{I} during registration such that only the spatial intensity differences due to structural deformation caused by mass effect are recovered, when compared to \mathcal{I}_{Atlas} . Given the reference (\mathcal{I}) and floating (\mathcal{I}_{Atlas}), the non-rigid alignment can be formulated as: $(\mathcal{I}, \hat{\mathcal{I}}_{mask}) = T(\mathcal{I}_{Atlas})$ where, $T(\cdot)$ is the forward transformation of the composite (including affine components) voxel-wise deformation field that maps the displacements of the voxels between the reference and floating volumes. This transformation also propagates the atlas brain mask ($\hat{\mathcal{I}}_{Atlas}$) to the subject space, thereby skull-stripping the subjects. As ANTs SyN satisfies the conditions of a diffeomorphic registration, an inverse $T^{-1}(\cdot)$ exists, that successfully maps \mathcal{I} to the \mathcal{I}_{Atlas} space. This inverse mapping yields the tissue deformation of \mathcal{I} with respect to \mathcal{I}_{Atlas} , representing the deformations exerted on every $c \in C_N$, due to the tumor mass effect. Considering (c'_x, c'_y, c'_z) as new voxel positions of \mathcal{I} when mapped to \mathcal{I}_{Atlas} , the displacement vector is given as $[\delta x, \delta y, \delta z]$

where vector $(c'_x, c'_y, c'_z) = (c_x, c_y, c_z) + (\delta x, \delta y, \delta z)$, and the magnitude of deformation is given by: $D(c) = \sqrt{(\delta x)^2 + (\delta y)^2 + (\delta z)^2}$, for every $c \in C_N^j$, and $j \in \{1, \dots, k\}$. First order statistics (i.e. mean, median, standard deviation, skewness, and kurtosis) are then computed by aggregating $D(c)$ for every c within every sub-volume \mathcal{I}_N^j yielding a feature descriptor \mathbb{F}_{def}^j for every annular sub-region C_N^j , where $C_N^j \subset C_N$, $j \in \{1, \dots, k\}$.

2. **Extraction of 3D gradient-based descriptors from tumor, and peritumoral regions:** We used a 3D gradient-based texture descriptor presented in [3]. This texture descriptor captures tumor heterogeneity by computing higher order statistics from the gradient orientation changes computed across X , Y , and Z directions. These features has been shown to be successful in tumor characterization for a variety of applications in brain, lung and breast cancers. Briefly, for every $c \in [C_P, C_T]$, gradients along the X , Y and Z directions are computed as, $\nabla f(c) = \frac{\partial f(c)}{\partial X} \hat{i} + \frac{\partial f(c)}{\partial Y} \hat{j} + \frac{\partial f(c)}{\partial Z} \hat{k}$, where $\frac{\partial f(c)}{\partial q}$ is the gradient magnitude along the q axis, $q \in \{X, Y, Z\}$. A $N \times N \times N$ window centered around every $c \in C$ is selected to compute the localized gradient field. We then compute $\partial f_X(c_t)$, $\partial f_Y(c_t)$ and $\partial f_Z(c_t)$, for every $c \in [C_P, C_T]$, $t \in \{1, 2, \dots, N^3\}$. The vector gradient matrix \mathcal{F} associated with every c is given by $\mathcal{F} = [\partial f_X(c_t) \ \partial f_Y(c_t) \ \partial f_Z(c_t)]$, where $[\partial f_X(c_t) \ \partial f_Y(c_t) \ \partial f_Z(c_t)]$, $t \in \{1, 2, \dots, N^3\}$ is the matrix of gradient vectors in the X , Y and Z directions for every c_t given by a $N^3 \times 3$ matrix. Singular value decomposition of \mathcal{F} for a voxel c_t yields three dominant principal components $\psi_X(c_t)$, $\psi_Y(c_t)$ and $\psi_Z(c_t)$ in the X -, Y - and Z -directions respectively. Two principal orientations $\theta(c_t)$ and $\phi(c_t)$ can then be obtained to capture variability in orientations across (X, Y) , and (X, Y, Z) (in-plane and out-of-plane variability), given by $\theta(c_t) = \tan^{-1} \frac{\psi_Y(c_t)}{\psi_X(c_t)}$ and $\phi(c_t) = \tan^{-1} \frac{\psi_Z(c_t)}{\sqrt{\psi_Y^2(c_t) + \psi_X^2(c_t)}}$. Two separate $\mathcal{N} \times \mathcal{N}$ co-occurrence matrices, \mathcal{M}^θ , and \mathcal{M}^ϕ are computed, corresponding to $\theta(c_t)$ and $\phi(c_t)$, which capture the orientation pairs between voxels in a local neighborhood. We then individually compute 13 Haralick statistics as $[\mathcal{S}_{\theta_b}, \mathcal{S}_{\phi_b}]$, $b \in [1, 13]$ from \mathcal{M}^θ and \mathcal{M}^ϕ , for every voxel $c \in \{C_P, C_T\}$ as shown in [11]. For every b , first order statistics (i.e. mean, median, standard deviation, skewness, and kurtosis) are then computed by aggregating $[\mathcal{S}_{\theta_b}, \mathcal{S}_{\phi_b}]$ for every $c \in \{C_P, C_T\}$ yielding a feature descriptor \mathbb{F}_{tex}^T for the tumor volume, and \mathbb{F}_{tex}^P for the peri-tumoral volume.
3. **Computation of r-DepTH descriptor:** The descriptor \mathbb{F}_{depth} is obtained as a feature vector by concatenation of the deformation descriptor, \mathbb{F}_{def} , and the texture descriptors, \mathbb{F}_{tex}^T , and \mathbb{F}_{tex}^P .

4 Experimental Design

4.1 Data Description and Preprocessing

A total of 105 3-Tesla treatment-naive Gadolinium (Gd)-contrast T1w, T2w, and FLAIR MRI GBM studies were retrospectively obtained from the Cancer

Imaging Archive [12]. We restricted our inclusion criteria to include short-term survivors with an overall survival (OS) of <240 days and long-term survivors with OS > 540 days. This resulted in a total of 68 patients in the training cohort, with an equal split of 34 STS and LTS cases respectively. An independent cohort of a total of 11 studies (4 LTS and 7 STS cases), with the same MRI sequences as the training set, was obtained from the collaborating institution. The T1w images were first bias-corrected using N4 bias correction [13]. The lesion masks were manually delineated by an expert radiologist as tumor, peri-tumoral, and normal parenchymal regions on T1w MRI scans.

4.2 Implementation Details

The normal parenchymal region was divided into $k = 12$ annual bands, such that neighboring bands were equidistant to each other at 5 mm. Hence, each brain MRI volume \mathcal{I} is associated with a 60×1 deformation feature vector \mathbb{F}_{def} , with a total of 5 statistics (mean, median, standard deviation, skewness, and kurtosis) obtained from each k , $k \in [1, \dots, 12]$. Similarly for \mathbb{F}_{tex}^T and \mathbb{F}_{tex}^P respectively, the same 5 statistics are computed from $[\mathcal{S}_{\theta_b}, \mathcal{S}_{\phi_b}]$, $|\mathcal{S}_{\theta_b}| = |\mathcal{S}_{\phi_b}| = 13$, resulting in a 130×1 feature vector, each. Following feature extraction, sequential forward feature selection [14] was employed to identify the most discriminating subset of features between STS and LTS from the training cohort. A total of 50 iterations of three-fold (one fold held-out for testing), patient-stratified, cross-validation scheme was used for constructing a linear discriminant analysis (LDA) classifier using the training set. The top 5 best performing features were obtained for each of the four feature sets, \mathbb{F}_{def} , \mathbb{F}_{tex}^P , \mathbb{F}_{tex}^T , and \mathbb{F}_{depth} using the training cohort. Additionally, a total of 6 shape features (\mathbb{F}_{shape}) were also extracted for every \mathcal{I} for comparison with the other 4 feature sets. The top performing features from each of the 5 feature sets were used to lock down five different LDA classifiers, and independently evaluated on the $N = 11$ test cases. Kaplan-Meier (KM) survival analysis, along with log-rank test, was independently employed for each of the 5 feature sets, to compare survival times between the two groups (STS versus LTS). The horizontal axis on the KM curve shows the time in days from initial

Table 1. List of features computed from T1w scans to distinguish LTS from STS.

Feature	#	Description
\mathbb{F}_{def}	60	Mean, Median, Std, skewness, kurtosis within each 5 mm annular region in N
$\mathbb{F}_{tex}^P, \mathbb{F}_{tex}^T$	130	Five first order statistics of Entropy, Energy, Inertia, IDM, Correlation, Info1, Info2, Sum Average, Sum Variance, Sum Entropy, Difference average, Difference variance, Differential entropy
\mathbb{F}_{shape}	6	Volume, major and minor axis length, eccentricity, orientation, compactness

diagnosis, and the vertical axis shows the probability of survival. Any point on the curve reflects the probability that a patient in each group would remain alive at that instance. Labels assigned by the LDA classifier were used for KM-curve generation (Fig. 4).

5 Results and Discussion

5.1 Distinguishing LTS vs STS Using r-DepTH

The analysis on the training dataset on \mathbb{F}_{def} demonstrated that the skewness of deformation magnitude across LTS (Fig. 3(a)) and STS (Fig. 3(b)) was consistently statistically significantly different ($p \leq 0.05$) for annular regions $g \leq 30$ millimeters proximal to the tumor (Fig. 3(c), (d)). However, the significance did not hold for $g > 30$ mm across LTS and STS studies. Higher values of skewness are shown in red while lower values are shown in dark blue in Fig. 3. Deformation magnitudes were found to be highly positively skewed (shown in red) in STS as compared to LTS (3(e)) (shown in green). Our results corroborate with recent findings in [15], suggesting that there may be prognostic impact due to tumor burden in certain cognitive areas because of the structural deformation heterogeneity, eventually affecting survival. Further, the top 5 features on the training set ($N = 68$) across \mathbb{F}_{def} , \mathbb{F}_{tex} and \mathbb{F}_{depth} , yielded an AUC of 0.71 ± 0.08 , 0.77 ± 0.08 and 0.83 ± 0.07 respectively via a 3-fold cross-validation.

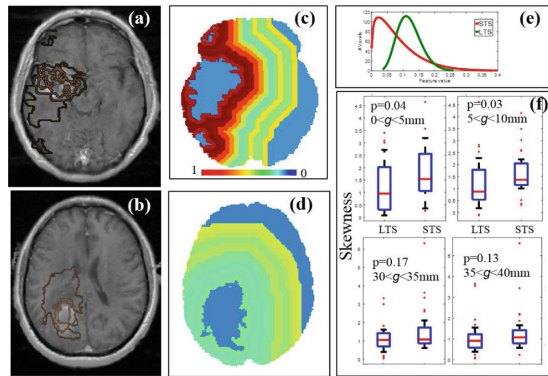


Fig. 3. T1w scans of two different STS (a) and LTS patients (b). Figures 3(c), (d) show the corresponding deformation skewness statistics within 5 mm-annular regions in the normal parenchyma. Histograms of the deformation magnitudes in the first annular band between LTS and STS are shown in (e). Deformation magnitudes were found to be highly positively skewed in STS as compared to LTS. Box plots of deformation skewness across 4 different annular bands, $g \leq 5$, $5 < g \leq 10$, $30 < g \leq 35$, $35 < g \leq 40$ (in mm) are shown in (f).

5.2 Evaluation on Independent Validation Set

Figure 4(a) shows the ideal “ground truth” KM curve for STS and LTS patients obtained on an independent cohort of ($N = 11$) studies. Figures 4(b)–(d) show the KM curves obtained using the assigned labels from the LDA classifier using \mathbb{F}_{def} , \mathbb{F}_{tex} and \mathbb{F}_{depth} respectively. KM curves using \mathbb{F}_{def} ($p=0.176$), \mathbb{F}_{tex} ($p = 0.81$), \mathbb{F}_{shape} ($p = 0.1$) alone to distinguish LTS and STS patients, were not found to be significant. However, interestingly, \mathbb{F}_{depth} descriptor, yielded a statistically significant survival curve for distinguishing STS versus LTS with $p = 0.038$. Additionally, the classifier trained on \mathbb{F}_{depth} could correctly predict the survival group in 9 out of the 11 studies (accuracy = 81%), while \mathbb{F}_{tex}^T achieved an accuracy of 64%, and \mathbb{F}_{tex}^P of 54% in predicting the survival group.

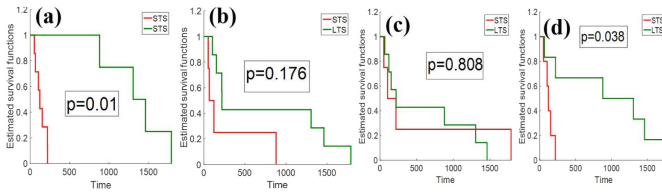


Fig. 4. KM curves obtained from the validation set ($N = 11$) are shown for ground truth (a), \mathbb{F}_{def} (b), \mathbb{F}_{tex} (c), and (d) \mathbb{F}_{depth} respectively.

6 Concluding Remarks

In this study, we present a new radiomics approach, r-DepTH, which comprehensively captures the intra-, and extra-tumoral heterogeneity by measuring (a) the anatomical deformations in surrounding normal parenchyma, and (b) the gradient-based texture representations from within the tumor. The r-DepTH features demonstrated significant improvement in predicting overall survival in GBM patients using KM curve analysis ($p = 0.038$), over employing deformation and texture features alone. Future work will focus on validating r-DepTH on a larger cohort of studies to establish its efficacy as a new prognostic marker for GBM as well as other solid tumors. We will further employ r-DepTH in conjunction with other known clinical variables, to reliably predict patient outcome and improve treatment management in solid tumors.

References

1. Chai, H., et al.: Field effect in cancer: an update. *Ann. Clin. Lab. Sci.* **39**(4), 331–337 (2009)
2. Silbergeld, D.L., et al.: The cause of death in patients with glioblastoma is multifactorial. *J. Neuro-Oncol.* **10**(2), 179–185 (1991)

3. Prasanna, P., et al.: Co-occurrence of local anisotropic gradient orientations (collage): a new radiomics descriptor. *Sci. Rep.* **6** (2016)
4. Aerts, H., et al.: Decoding tumour phenotype by noninvasive imaging using a quantitative radiomics approach. *Nat. Commun.* **5** (2014)
5. Chaddad, A., et al.: Radiomic analysis of multi-contrast brain MRI for the prediction of survival in patients with glioblastoma multiforme. In: EMBS (2016)
6. Tiwari, P., et al.: Computer-extracted texture features to distinguish cerebral radionecrosis from recurrent brain tumors on multiparametric MRI: a feasibility study. *Am. J. Neuroradiol.* **37**(12), 2231–2236 (2016)
7. Prasanna, P., et al.: Radiomic features from the peritumoral brain parenchyma on treatment-naive multi-parametric MR imaging predict long versus short-term survival in glioblastoma multiforme: preliminary findings. *Eur. Radiol.*, 1–10 (2016)
8. Salazar, O., et al.: The spread of glioblastoma multiforme as a determining factor in the radiation treated volume. *Radiat. Oncol.* Biol.* Phys.* **1**(7–8), 627–637 (1976)
9. Hu, L.S., et al.: Radiogenomics to characterize regional genetic heterogeneity in glioblastoma. *Neuro-Oncol.* **19**(1), 128–137 (2017)
10. Avants, B.B., et al.: Symmetric diffeomorphic image registration with cross-correlation: evaluating automated labeling of elderly and neurodegenerative brain. *Med. Image Anal.* **12**(1), 26–41 (2008)
11. Haralick, R.M., et al.: Textural features for image classification. *Syst. Man Cyber.* **6**, 610–621 (1973)
12. Clark, K., et al.: The cancer imaging archive (TCIA): maintaining and operating a public information repository. *J. Digit. Imaging* **26**(6), 1045–1057 (2013)
13. Tustison, N.J., et al.: N4ITK: improved N3 bias correction. *IEEE TMI* **29**(6), 1310–1320 (2010)
14. Tang, J., et al.: Feature selection for classification: a review. *Data Classif.: Algorithms Appl.* (2014)
15. Liu, L., Zhang, H., Rekić, I., Chen, X., Wang, Q., Shen, D.: Outcome prediction for patient with high-grade gliomas from brain functional and structural networks. In: Ourselin, S., Joskowicz, L., Sabuncu, M.R., Unal, G., Wells, W. (eds.) MICCAI 2016. LNCS, vol. 9901, pp. 26–34. Springer, Cham (2016). doi:[10.1007/978-3-319-46723-8_4](https://doi.org/10.1007/978-3-319-46723-8_4)